반도체디스플레이기술학회지 제23권 제2호(2024년 6월)
Journal of the Semiconductor & Display Technology, Vol. 23, No. 2. June 2024.

An Experimental Study on IMP-based and DOB-based Controllers for Position Control of a BLDC Motor System

Dong Cheol Song[*], Seung Tae Hwang[*], Nebiyeleul Daniel Amare[*] and Young Ik Son[*†]
[*†] Department of Electrical Engineering, Myongji University

ABSTRACT

As semiconductor processes require several nanometers precision, the importance of motor control is increasing in semiconductor equipment. Due to unpredictable uncertainties such as friction and mechanical vibrations achieving precise position control in semiconductor processes is challenging. The internal model principle-based controller is a control technique that ensures robust steady-state performance by incorporating a model of the reference and disturbance. The disturbance observer-based controller is a prominent robust control technique implemented to cope with various nonlinearities and uncertainties. Provided that the two controllers can be designed to exhibit equivalent performance under certain conditions, this paper demonstrates through experiments that they yield identical results for the case of a BLDC position control problem. The experimental results also indicate that they can offer enhanced robustness compared with the conventional PID controller in the presence of a time-varying disturbance.

Key Words : Semiconductor Equipment, BLDC Motor Control, Internal Model Principle, Disturbance Observer, Reduced-order Observer, Ramp Reference Signal

1. Introduction

The demand of high-precision position control systems in the semiconductor manufacturing industry is an imparative that grows as the semiconductor device miniaturization continues. For a high-precision position control system of semiconductor equipment, robust motor control against disturbance is essential. For example, wafer scanners, the primary equipment of the photo process, use linear motors to position wafers and reticles. Achieving fast and accurate positional alignment necessitates compensating for disturbance such as force ripple or structural vibrations, which in turn requires advanced control algorithms [1,2]. Other factors such as limit cycles, often caused by backlash between the motor and stage, complicate precise control and require the implementation of robust control technique to mitigate their effect [3]. Therefore, motor control of semiconductor equipment is one of the important factors in the semiconductor industry and requires accurate position control and effective disturbances compensation.

The motor used in the semiconductor process is important not only for precision, but also for durability and safety. The BLDC motor has advantages of high efficiency and high starting torque. In addition, it uses an electronic rectification method without a commutator, so it has less failure or wear and is advantageous for noise and vibration. The BLDC motor may have reduced accuracy due to the uncertainty of electrical/mechanical system parameters, friction and disturbance. As a result, various advanced control algorithms have been proposed in control systems literature for precise position control. Among them in [4], SOSMO (Second-order Sliding Mode Observer) was presented, and in [5], IMC (Internal Model Control) PID control technique based on MLESO (Model Linear Extended State Observer) was applied. In addition, disturbance observer-based control methods [6-10] or control methods based on internal model principle [11-13] are

[†]E-mail: sonyi@mju.ac.kr

being actively studied as robust control techniques.

Meanwhile, in the preceding study [14], design conditions to ensure that the internal model principle (IMP) -based controller and the reduced-order observer (RODOB) -based controller have the same performance in the DC motor position control system were presented, and the results were confirmed through simulation for the case where the reference and disturbance were sinusoidal functions. In this paper, we validate the findings of previous studies by applying them to a more practical and complex BLDC motor position control system, specifically examining a reference and disturbance consisting of a constant term and a ramp term.

The paper is organized as follows. In Section 2.1, the control system is defined, and in Sections 2.2 and 2.3, IMP-based and RODOB-based controllers are introduced and designed to have equivalence. Section 3.1 introduces the experimental environment, and Section 3.2 introduces a simple modeling method through open-loop experiments in situations where it is difficult to apply existing motor model equations. In Sections 3.3 and 3.4, the position control performance of the two controllers is compared through simulation and experiment, and the conclusion is presented in Section 4.

2. System Model and Controller Design

2.1 System Model

This paper deals with a three-phase BLDC motor equation given as [15]

$$\begin{bmatrix} v_a \\ v_b \\ v_c \end{bmatrix} = \begin{bmatrix} R_a & 0 & 0 \\ 0 & R_a & 0 \\ 0 & 0 & R_a \end{bmatrix} \begin{bmatrix} i_a \\ i_b \\ i_c \end{bmatrix} + \begin{bmatrix} L_s - M & 0 & 0 \\ 0 & L_s - M & 0 \\ 0 & 0 & L_s - M \end{bmatrix} \frac{d}{dt} \begin{bmatrix} i_a \\ i_b \\ i_c \end{bmatrix} + \begin{bmatrix} e_a \\ e_b \\ e_c \end{bmatrix}, \quad (1)$$

$$T_e - T_L = J\frac{d}{dt}\omega_m + B\omega_m$$

where v_a, v_b and v_c are phase voltages of BLDC motor, and R_a is the armature resistance. i_a, i_b and i_c are phase currents of BLDC motor, and L_s and M denote the self-inductance and mutual-inductance. e_a, e_b and e_c represent the back EMF of BLDC motor. T_e is the torque generated by the motor and ω_m is the speed of motor. J and B mean the moment of inertia and friction coefficient as seen from the motor shaft, and T_L denotes the load torque disturbance. The BLDC motor control system considering d-q transformation is as shown Fig. 1.

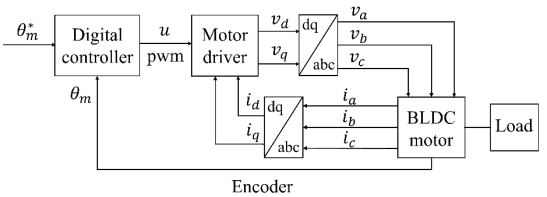

Fig. 1. BLDC motor position control system.

The BLDC motor system equation considering only the q-axis by d-q transformation of equation (1) is as follows.

$$\begin{aligned} &\frac{d}{dt}\theta_m = \omega_m, \\ &\frac{d}{dt}\omega_m = -\frac{B}{J}\omega_m + \frac{K_t}{J}i_q - \frac{1}{J}T_L, \\ &\frac{d}{dt}i_q = -\frac{K_b}{L_a}\omega_m - \frac{R_a}{L_a}i_q + \frac{1}{L_a}u. \end{aligned} \quad (2)$$

In equation (2), θ_m and i_q are the angle and q-axis current of the motor. u denotes the voltage input. K_t, K_b and L_a denote the torque constant, back EMF constant and the armature inductance, where $L_a = L_s - M$.

Generally, the electrical dynamic characteristic of the motor is very fast compared to the mechanical dynamic characteristic, as such this paper deals with the reduced model with $L_a \approx 0$ as shown in equation (3) [16,17].

$$\frac{d}{dt}\theta_m = \omega_m, \quad (3a)$$

$$\frac{d}{dt}\omega_m = -\frac{BR_a + K_tK_b}{JR_a}\omega_m + \frac{K_t}{JR_a}u - \frac{1}{J}T_L. \quad (3b)$$

For notation simplicity, we define the state of system $x = [\theta_m;\ \omega_m]$ and disturbance $d = -(R_a/K_t)/T_L$, the following equation can be obtained.

$$\begin{aligned} &\dot{x} = Ax + B(u + d), A \in \mathbb{R}^{2\times2}, B \in \mathbb{R}^{2\times1}, \\ &r = r_0 + r_1 t, \\ &d = d_0 + d_1 t, \\ &y = Cx = x_1 = \theta_m. \end{aligned} \quad (4)$$

The position reference r and disturbance d considered in this paper consist of the sum of the constant term and the ramp term. d_0 and d_1 are the unknown constant.

The next section introduces IMP-based controller that includes the model of reference and disturbance.

2.2 IMP-Based Controller

This section deals with the control system as shown in Fig. 2. The error $E(s) = R(s) - Y(s)$ is as follows.

$$E(s) = \frac{1}{1 + C_1(s)G(s)}R(s) - \frac{G(s)}{1 + C_1(s)G(s)}D(s). \tag{5}$$

When all the roots of the characteristic equation $\gamma_1(s) := 1 + C_1(s)G(s) = 0$ are located in the LHP (Left Half Plane) region and the denominator of the controller $C_1(s)$ includes the characteristic polynomial of the reference and disturbance, the steady state error e_{ss} of the output can be made 0 [18]. In this way, if the controller includes characteristic polynomial of the reference and disturbance, in other words the model, a principle that can secure robust steady-state performance is called the internal model principle [11,19]. From equation (4), it can be seen that the characteristic polynomial of the reference and disturbance is s^2 and if the denominator of the controller $C_1(s)$ includes s^2 as an argument according to the internal model principle, a control result with a steady state error of 0 can be obtained.

The controller $C_1(s)$ including the model of reference and disturbance is shown in equation (6).

$$C_1(s) = \frac{\beta_3 s^3 + \beta_2 s^2 + \beta_1 s + \beta_0}{s^2(s + \alpha)} \tag{6}$$

where the controller parameters β_i $(0 \le i \le 3)$ and α are determined in consideration of the stability and transient performance of the closed loop transfer function.

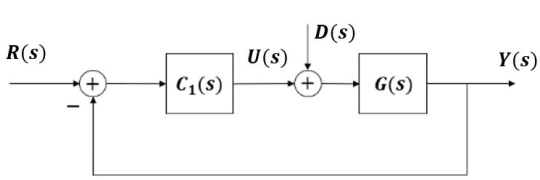

Fig. 2. Block diagram for IMP-based control system.

The next section introduces a disturbance observer-based controller with robust control performance by compensating for disturbance using a disturbance model.

2.3 RODOB-Based Controller

In this section, we design the RODOB-based controller for robustness against disturbance. First, for the observer design, the state-space equation matrix A_ξ and C_ξ for disturbance d in (4) are defined as follows.

$$\begin{bmatrix}\dot{\xi}_1 \\ \dot{\xi}_2\end{bmatrix} = \begin{bmatrix}0 & 1 \\ 0 & 0\end{bmatrix}\begin{bmatrix}\xi_1 \\ \xi_2\end{bmatrix} =: A_\xi \xi, \xi \in \mathbb{R}^2, \quad d = \xi_1 =: C_\xi \xi. \tag{7}$$

The extended system equation including disturbance is obtained using equation (7) as follows.

$$\begin{bmatrix}\dot{x} \\ \dot{\xi}\end{bmatrix} = \begin{bmatrix}A & BC_\xi \\ 0 & A_\xi\end{bmatrix}\begin{bmatrix}x \\ \xi\end{bmatrix} + \begin{bmatrix}B \\ 0\end{bmatrix}u =: \bar{A}z + \bar{B}u, \quad y = [C \quad 0_{1\times 2}]\begin{bmatrix}x \\ \xi\end{bmatrix} =: \bar{C}z. \tag{8}$$

In the above equation, the states of the extended system are $z = [x;\ \xi] \in \mathbb{R}^4$, system matrix $\bar{A} \in \mathbb{R}^{4\times 4}$, input matrix $\bar{B} \in \mathbb{R}^{4\times 1}$ and output matrix $\bar{C} \in \mathbb{R}^{1\times 4}$. It can be seen that the extended system (8) is observable [20]. The first component of state z is the system output y, and the remaining states ω_m, ξ_1 and ξ_2 are defined as z_2 that is to be estimated. For RODOB design, equation (8) is rewritten as follows.

$$\dot{z}_1 = a_{11}z_1 + \bar{A}_{12}z_2 + \bar{B}_1 u, \quad \dot{z}_2 = \bar{A}_{21}z_1 + \bar{A}_{22}z_2 + \bar{B}_2 u, \quad y = z_1 = [1 \quad 0 \quad 0 \quad 0]z \tag{9}$$

where $z_1 = \theta_m$, $z_2 = [\omega_m \quad \xi^T]^T$, $a_{11} = 0$, $\bar{A}_{12} = [1 \quad 0 \quad 0]$ and $\bar{B}_1 = 0$ when compared to equation (3a). With equation (9) RODOB is designed as follows.

$$\dot{\hat{z}}_2 = \bar{A}_{21}z_1 + \bar{A}_{22}\hat{z}_2 + \bar{B}_2 u + L(\bar{A}_{12}z_2 - \bar{A}_{12}\hat{z}_2) + Mr \tag{10}$$

where Mr is added for the design of the controller equivalent to equation (6). The observer gain $L = [l_1 \quad l_2 \quad l_3]^T$ is designed such that the matrix $A_o (=: \bar{A}_{22} - L\bar{A}_{12})$ is a Hurwitz matrix.

From equations (9) and (10), the dynamic characteristics of the estimated error $\tilde{z}_2 := z_2 - \hat{z}_2$ can be expressed as follows.

$$\dot{\tilde{z}}_2 = A_0\tilde{z}_2 - Mr,\ A_o = \bar{A}_{22} - L\bar{A}_{12}\,. \tag{11}$$

To avoid the use of the differential value ($\dot{z}_1$) included in $\bar{A}_{12}z_2$ of equation (10), we can define variable $z_c =: \hat{z}_2 - Lz_1$ and the following observer equation can be obtained.

$$\begin{aligned}\dot{z}_c = A_0 z_c + (\bar{A}_{21} - La_{11} + A_0L)z_1 \\ +(\bar{B}_2 - L\bar{B}_1)u + Mr\,.\end{aligned} \tag{12}$$

The RODOB-based control system structure is shown in Fig. 3. In the figure, N and M are gains multiplied by the reference, and $\bar{K}$ is the control gain for the estimated state and disturbance.

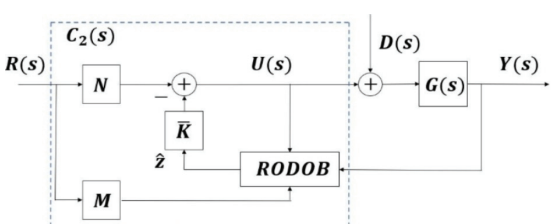

Fig. 3. Block diagram for RODOB-based control system.

When the variable $\hat{z} =: \begin{bmatrix} z_1 & \hat{z}_2{}^T \end{bmatrix}^T$ of the RODOB, the controller in Fig. 3 is as follows.

$$\begin{aligned} &u = Nr - \bar{K}\hat{z}, \\ &\bar{K} = [K \quad C_\xi] = [k_1 \quad k_2 \quad C_\xi],\ \bar{K}_2 = [k_2 \quad C_\xi]. \end{aligned} \tag{13}$$

When N, M is determined as follows, the RODOB-based controller in Fig. 3 has the same structure and transfer function as the IMP-based controller (6) in Fig. 2 [12].

$$\begin{aligned} &N = k_1 + \bar{K}_2 L\,, \\ &M = -(\bar{A}_{21} - La_{11} + A_oL)\,. \end{aligned} \tag{14}$$

The controller $C_2(s)$ designed is as follows.

$$C_2(s) = \left(1 + \bar{K}_2G_2(s)\right)^{-1}\left(N + \bar{K}_2G_1(s)\right). \tag{15}$$

When the gains K and L are determined so that the two control systems Fig. 2 and Fig. 3 have the same structure and closed-loop characteristic equation, the same RODOB-based controller as the IMP-based controller can be obtained by determining N and M as shown in equation (14). In this paper, we first design the RODOB-based controller $C_2(s)$ and then determine the gains α, β of the IMP-based controller $C_1(s)$ through parameter comparison.

3. Experiments

This section introduces the experimental environment and obtains the transfer function of the system to be controlled through the open-loop experiment. In addition, the performance of the two controllers is compared through simulation and experiment.

3.1 Experimental Environment

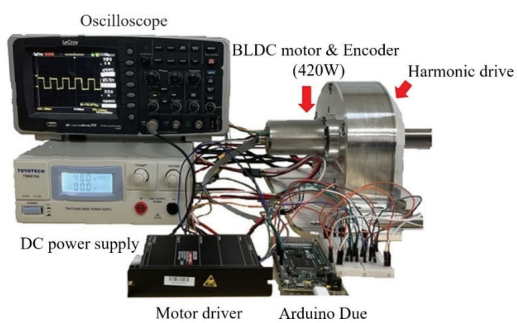

Fig. 4. BLDC motor control system for experiments.

The experimental equipment is shown in Fig. 4. The power supplied from the DC power supply is converted into a control input voltage through a motor driver. The Arduino Due receives the encoder pulse signal to create a PWM control input and transmits it to the motor driver. The motor driver used in the experiment is Maxon's ESCON 70/10, which supports speed PI control. For advanced control such as IMP-based control, this experiment performs speed control by PWM method using a digital controller, and at this time, PWM is converted into speed reference. The block diagram for the experimental

environment is shown in Fig. 5, and the main specifications of the experimental equipment are shown in Table 1-4 [21,22].

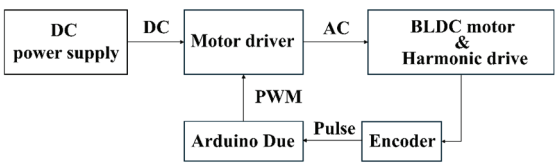

Fig. 5. Block diagram for experiments.

Table 1. BLDC motor specification (EC-i 52)

Power	420W
Nominal voltage	48V
Nominal current	9.87A
Nominal speed	3990rpm

Table 2. Encoder specification (Encoder 16 RIO)

PPR	32768
Number of channels	3
Max. operating frequency	3125kHz

Table 3. Motor driver specification (ESCON 70/10)

Nominal operating voltage	10~70VDC
Output current	10A
Max PWM frequency	5kHz

Table 4. Arduino Due specification

MCU type	32-bit ARM Coretex-M3
Operating voltage	3.3V
Clock speed	84MHz

3.2 System Transfer Function

This section finds the nominal transfer function of the system via a step response experiment. Equation (3b) can be given by

$$\frac{d}{dt}\omega_m = -\frac{1}{\tau}\omega_m + \frac{k}{\tau}u \tag{16}$$

where $\tau = (JR_a)/(BR_a + K_tK_b)$ and $k = (JR_a)/K_t$.

Since it is practically not easy to obtain J and B reflecting the moment of inertia and the coefficient of friction of the load in an experiment, τ and k are obtained through experiments. In the open-loop experiment, the system input u is set as a speed input in consideration of the characteristics of the motor driver. At this time, the unit of ω_m and u is rpm. A step input $u = 573$ is applied to make the output speed steady state $\omega_{ss} = 300$. The final value of the output is determined by considering the experimental environment and the maximum value of the allowable current. Fig. 6 is the result of the open-loop experiment. The time constant τ is the time when the output is 63% (=189) of the steady state and the average value through a total of 5 repetitions is used. The constant k is determined using the final value theorem as follows.

$$\begin{aligned}\omega_{ss} &= \lim_{t\to\infty}\omega(t) = \lim_{s\to 0} s \times \Omega(s) \\ &= \lim_{s\to 0} s \times \frac{k}{\tau s + 1} \times \frac{573}{s} = 573k\,.\end{aligned} \tag{17}$$

The experimental results are $\tau = 0.0346[s]$, $k = 0.5236$.

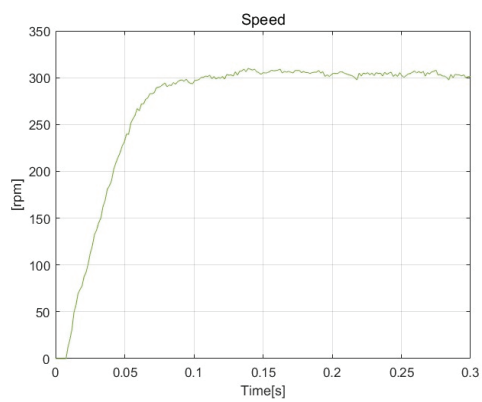

Fig. 6. Open-loop control output.

The next section introduces simulations of IMP-based and RODOB-based controllers using the system transfer functions obtained in this section.

3.3 Simulations

The reference r and disturbance d used in the simulations consist of a constant and a ramp function as shown in Fig. 7. The disturbance is applied from 6 seconds. RODOB-based controller is first designed to determine the gains α, β of the IMP-based controller. The poles of the

closed loop transfer function considered are determined as follows.

$$s = -3 \pm j3, -30 \pm j50, -40\,. \tag{18}$$

The parameters K, N, L and M are obtained as follows.

$$K = [0.1982 \quad -0.2522]\,, N = 46.1435\,,$$
$$L = \begin{bmatrix} 0.711e+2 \\ 0.639e+2 \\ 1.4978e+3 \end{bmatrix},\ M = \begin{bmatrix} 0.131e+4 \\ 0.304e+4 \\ 1.0649e+5 \end{bmatrix}. \tag{19}$$

The IMP-based controller equivalent to the RODOB-based controller designed from equations (15) and (18) is as follows.

$$C_1(s) = \frac{\beta_3 s^3 + \beta_2 s^2 + \beta_1 s + \beta_0}{s^2(s + 77.0983)}. \tag{20}$$

In the above equation, $\beta_3 = 46.1435$, $\beta_2 = 1.9009e+03$, $\beta_1 = 1.0137e+04$, $\beta_0 = 2.6961e+04$.

To compare the performance of the two controllers, a PID controller is also considered in this section.

$$C_3(s) = \frac{K_d s^2 + K_p s + K_i}{s}. \tag{21}$$

The gains K_p, K_i, K_d are determined so that the poles of the closed loop transfer function were -3, -30 and -40. They are given by $K_p = 15.5290$, $K_i = 39.6486$, and $K_d = 0.4857$.

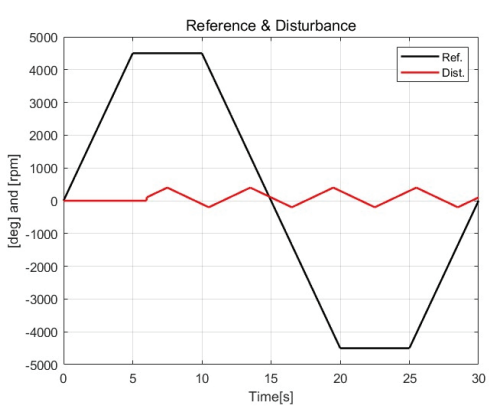

Fig. 7. Reference & Disturbance.

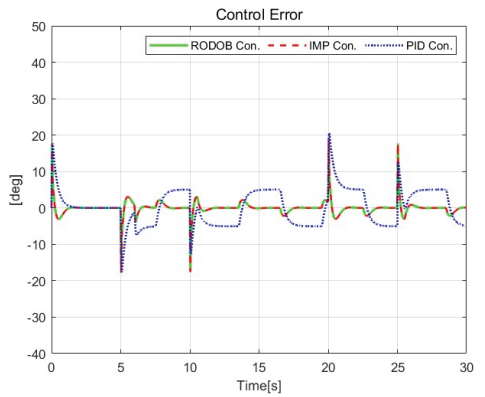

Fig. 8. Control error (simulation).

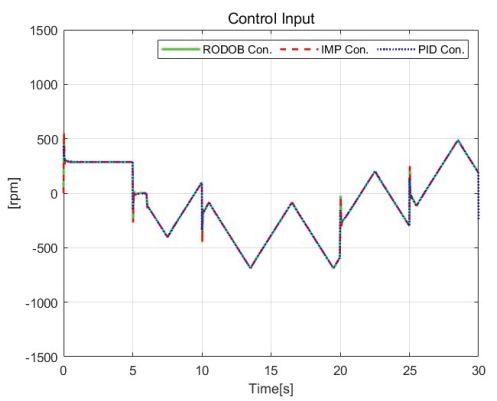

Fig. 9. Control input (simulation).

Fig. 7 shows the reference (Ref.) and disturbance (Dist.) used both in the simulations and the experiments of the next section. Fig. 8 and Fig. 9 show the control error and control input. Unlike the PID controller the two controllers can accurately follow the reference without the steady state error. It can also be seen that the performance of the RODOB-based controller and the IMP-based controller are the same.

In the next section, experiments are conducted to confirm that the same results are obtained even in non-ideal situations.

3.4 Experiments

In this section, through experiments, it is checked whether the IMP-based controller and RODOB-based controller have the same results as the simulation. The reference, disturbance, controller parameters and gains used in the experiment are the same as those of the simulation.

In addition, the control period and the PWM period are 1ms and 0.2ms, respectively.

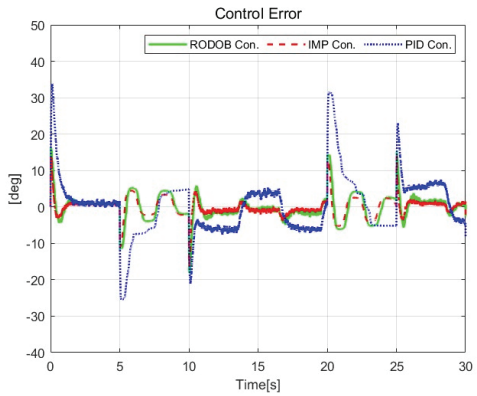

Fig. 10. Control error (experiment).

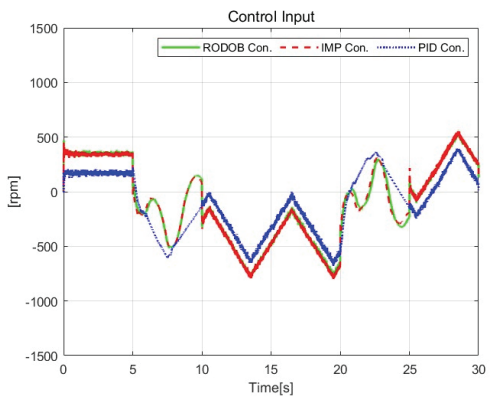

Fig. 11. Control input (experiment).

Fig. 10 is the control error and Fig. 11 is the control input. Fig. 10 shows that both the RODOB-based controller and the IMP-based controller follow the reference with high accuracy. Also, it can be seen that the two controllers have better transient and steady state performance compared to the PID controller when there is a disturbance and experimental uncertainties. While there is a difference in that the simulation is continuous time control and the experiment is discrete time control, it is confirmed that the previous two controllers are more robust against uncertainties than the conventional controller.

4. Conclusion

This paper deals with the problem of position control of BLDC motor under the disturbance consisting of a constant and a ramp signal. The experimental study presented in the paper, applied to a practical system, builds on previous theoretical work that established the equivalent conditions for the IMP-based controller and the RODOB-based controller. Through simulations and experiments, it was confirmed that the results of the two controllers show similar characteristics and offer better control performance compared with the conventional PID controller. In particular, it was confirmed that the two controllers provide more robustness than the PID controller in the presence of disturbance. The results presented in the paper are significant due to the presence of a motor driver with a built-in PI algorithm for speed control and a Harmonic driver with nonlinear friction in the experimental environment, which makes it more difficult to use the existing motor equation. Future works will explore experimental studies which consider operating characteristics of various semiconductor equipment.

Acknowledgement

This paper was conducted with the support of the Korea Institute for Advancement of Technology (G02P18800 005502) through the 2024 Ministry Collaborative Semiconductor Main Track Project, and the authors would like to thank Professor S. J. Hong of Myongji University for his help in carrying out the research.

References

1. S. Mishra, J. Coaplen, and M. Tomizuka, “Precision positioning of wafer scanners segmented iterative learning control for nonrepetitive disturbances [Applications of control],” IEEE Control Systems Magazine, vol. 27, no. 4, pp. 20-25, (2007).
2. K. C. Kim, J. J. Kim, Y. M. Choi, and D. G. Gweon, “Design of a hybrid controller to eliminate the force ripple in the linear motor,” J. of the Semiconductor & Display Technology, vol. 7, no. 1, pp. 17-22, (2008).
3. S. C. Ko and K. B. Jin, “The mechanical characteristic analysis and improvement of precision position control system with AC servo motor and ball screw,” J. of the Semiconductor & Display Technology, vol. 6, no. 1, pp. 31-36, (2007).
4. R. Yang, M. Wang, L. Li, Y. Zenggu, and J. Jiang, “Integrated uncertainty/disturbance compensation with second-order sliding-mode observer for PMLSM-driven motion stage,” IEEE Trans. Power Electron., vol. 34, no.

3, pp. 2597-2607, (2019).
5. Y. Liu, J. Gao, Y. Zhong, and L. Zhang, “Extended state observer-based IMC-PID tracking control of PMLSM servo systems,” IEEE Access, vol. 9, pp. 49036-49046, (2021).
6. Y. I. Son and I. H. Kim, “A robust state observer using multiple integrators for multivariable LTI systems,” IEICE Trans. Fund. Electron., vol. E93-A, no. 5, pp. 981-984, (2010).
7. M. Ruderman, A. Ruderman, and T. Bertram, “Observer-based compensation of additive periodic torque disturbances in permanent magnet motors,” IEEE Trans. Ind. Inf. vol. 9, no. 2, pp. 1130-1138, (2013).
8. Y. I. Son, I. H. Kim, D. S. Choi, and H. Shim, “Robust cascade control of electric motor drives using dual reduced-order PI observer,” IEEE Trans. Ind. Electron., vol. 62, no. 6, pp. 3672-3682, (2015).
9. I. H. Kim and Y. I. Son, “Design of a low-order harmonic disturbance observer with application to a DC motor position control,” energies, vol. 13, no. 5, pp. 1020, (2020).
10. Y. S. Cho, H. J. Choi, S. M. Jeon, J. H. Shin, J. Y. Lee, B. Lee, and Y. I. Son, “Trajectory tracking controller for semiconductor equipment motors based on PI observer,” J. of the Semiconductor & Display Technology, vol. 22, no. 2, pp. 96-103, (2023).
11. B. A. Francis and W. M. Wonham, “The internal model principle of control theory,” Automatica, vol. 12, no. 5, pp. 457-465, (1976).
12. Y. Joo, G. Park, J. Back, and H. Shim, “Embedding internal model in disturbance observer with robust stability,” IEEE Trans. Autom. Control, vol. 61, no. 10, pp. 3128- 3133, (2016).
13. J. I. Yuz and M. E. Salgado, “From classical to state-feedback-based controllers,” IEEE Control Systems Magazine, vol. 23, no. 4, pp. 58-67, (2003).
14. Y. I. Son and S. C. Lim, “A comparison of IMP-based and DOB-based controllers for a DC motor position control system,” Trans. of KIEE, vol. 73, no. 2, pp. 343-348, (2024).
15. S. H. Kim, Motor Control, Bokdu Publisher, 5th ed., pp 156-159, (2024).
16. J. Yao, Z. Jiao, and D. Ma, “Adaptive robust control of DC motors with extended state observer,” IEEE Trans. Ind, Electron., vol. 61, no. 7, pp. 3630-3636, (2014).
17. J. H. Yook, I. H. Kim, M. S. Han, and Y. I. Son, “Robustness improvement of DC motor speed control using communication disturbance observer under uncertain time delay,” Electron. Lett., vol. 53, no. 6, pp. 389-391, (2017).
18. Y. I. Son and S. J. Yang, “$e_{ss} = 0$: IMP-based controller,” KIPE Magazine, vol. 26, no. 1, pp. 64-69, (2021).
19. G. F. Franklin, J. D. Powell, and A. Emami-Naeini, Feedback Control of Dynamic Systems, 6th ed., Pearson, (2010).
20. T. Kailath, Linear Systems, Prentice Hall, Inc., (1980).
21. EC-i 52 and ESCON 70/10 details. May 19, 2024, from https://www.maxongroup.com/maxon/view/product/633919, (2021).
22. Arduino Due details. May 19, 2024, from https://docs.arduino.cc/hardware/due/, (2024).

접수일: 2024년 6월 5일, 심사일: 2024년 6월 17일,
게재확정일: 2024년 6월 21일